Mater Eng Res, 2019, 1(2): 45-55
DOI: 10.25082/MER.2019.02.003

RESEARCH ARTICLE

# Monitoring localized corrosion of Inconel 82 weld overlay on 304L SS weld by electrochemical noise

Girija Suresh[1*] Hemant Kumar[1]

**Abstract:** The manuscript presents the results from the electrochemical noise (EN) monitoring of Inconel 82 weld overlay on Type 304L stainless steel (SS) weld in 0.01M $FeCl_3$. The microstructure of the weld overlay obtained from optical and scanning electron microscopy (SEM) showed an austenite structure, containing equiaxed dendrites and secondary phases at the interdendritic region. Energy dispersive spectroscopy (EDS) attached to SEM revealed the secondary phases to be Nb rich Laves phase. The electrochemical potential noise was monitored using a three identical electrode configuration. The acquired signals were detrended, and wavelet analysis was employed to encode useful information from the noise transients. Visual examination of the potential noise-time record contained distinct high amplitude transients typical of localized corrosion attack. The energy distribution plots (EDP) of the potential noise derived from wavelet analysis depicted maximum relative energy on D6-D8 crystals, which represent large time scale events such as those occurring from localized attacks. Also, repassivation events too could be divulged from the potential EDP. The micrographs of the post electrochemical noise experimented specimens revealed the occurrence of localized attacks along the interdendritic region and none inside the dendritic cores. The presence of secondary phases along the interdendritic regions was found to be detrimental in chloride medium, imparting inferior localized corrosion resistance to the weld overlay.

**Keywords:** Inconel 82 weld overlay, 304L SS weld, electrochemical noise, localized corrosion, wavelet analysis

## 1 Introduction

Weld overlaying is a process, wherein, a compatible filler metal is deposited on a material surface by welding to achieve some desired property that is not intrinsic to the underlying material.[1] In the past, weld overlays were used as a band aid type of repair to address corrosion problems, but with the advances in automatic welding systems, weld overlaying of components has become a remedy to combat corrosion issues and to avoid costly and time consuming replacement of critical components. Ni-based superalloys have gained prominence in the recent past for application as weld overlays in petrochemical, oil and nuclear industry, and also in coal-fired boilers and waste to energy boilers to combat chloride and sulphide attack.[2–7] Weld overlays have been comprehensively employed over the globe to repair and mitigate stress corrosion cracking (SCC) in nuclear plant piping and nozzle welds.[5,6] In pressurized water reactors, low alloy steel components are joined to stainless-steel pipes using Inconel wires as they can accommodate compositional and thermal expansion variations of the dissimilar metals. Inconel 82, a Ni-Cr-Fe alloy, is often used as filler wire to join stainless steels and Ni-based superalloys in nuclear and petrochemical industries.[5–9] This filler wire is commercially employed for gas tungsten arc welding (GTAW), gas metal arc welding (GMAW), and submerged arc welding (SAW) of Inconel alloys 690, 600, and 601.[10] Weld metal that are deposited by Inconel 82 filler wire has high creep rupture strength at elevated temperatures, high tensile strength, good corrosion resistance and oxidation resistance.[10–13] Mortezaie *et al*.[12] have reported that Inconel 82 exhibited optimum mechanical properties and corrosion resistance for the dissimilar welding between Inconel 718 and 310 SS. Studies have revealed that Inconel 82 has superior intergranular corrosion resistance in boiling 25% nitric acid[13,14] and stress corrosion cracking resistance[15] than Inconel 182 and alloy 600.

304L SS is the main construction material in the back-

**Received:** April 30, 2019 **Accepted:** May 27, 2019; **Published:** May 30, 2019

*Correspondence to: Girija Suresh, Indira Gandhi Centre for Atomic Research, Kalpakkam, Tamilnadu 603102, India; Email: girija@igcar.gov.in
[1] Indira Gandhi Centre for Atomic Research, Kalpakkam, Tamilnadu 603102, India.

**Citation:** Suresh G and Kumar H. Monitoring localized corrosion of Inconel 82 weld overlay on 304L SS weld by electrochemical noise. *Mater Eng Res*, 2019, **1**(2): 45-55.

end of the Indian nuclear fuel cycle.[16,17] However, the weld region by virtue of its heterogenous microstructure, is highly susceptible to localized corrosion in the coastal environment. With Inconel 82 weld overlays gaining prominence worldwide to combat corrosion the cost effective way, it finds suitable application as a candidate material to protect the weld region of 304L SS from localized corrosion. Although the literature is replete in the microstructural characterization, mechanical properties and corrosion aspects of Inconel 82, much less information is reported on the localized corrosion mechanism of this material and their monitoring. Thus in this manuscript, an attempt is made to overlay Inconel 82 weld on 304L SS weld by the conventional and cost effective gas tungsten arc welding (GTAW) and to understand the localized corrosion mechanism of Inconel 82 weld overlay on 304L SS weld by using electrochemical noise (EN), which is an advanced corrosion monitoring technique in limelight for the past few decades, in particularly, to deduce localized corrosion. Electrochemical noise[18–22] is defined as the spontaneous and low frequency fluctuations of corrosion potential and corrosion current that occurs during a corrosion process and can be measured as potential noise and current noise respectively. EN fluctuations occur because of instantaneous variations in the rates of anodic and cathodic reactions during a corrosion event. The corrosion current noise and potential noise generated from various corrosion processes have distinct features, which can be continuously monitored to indicate the type of corrosion that makes EN an attractive tool for online corrosion monitoring[20–22] . The most attractive credential of this technique is that it does not require the application of an external potential, unlike other electrochemical techniques, and hence measurements can be made from naturally corroding surfaces[18] to obtain useful information on the type of corrosion and the rates as well. The advantage of EN over other corrosion monitoring techniques is well documented in the literature.[19,21] Though EN as a corrosion monitoring tool is well established since a few decades, there is no literature on its application for monitoring the corrosion of Inconel 82 weld overlays on 304L SS. In this manuscript, the results from EN monitoring of Inconel 82 weld overlay on 304L SS weld in chloride medium are presented. Wavelet analysis of the EN signal has been employed to decode information about the type of corrosion attack.

## 2 Experimental

The chemical composition of 304L SS base material, 308L SS filler wire and Inconel 82 filler wire used for the fabrication of the weld pad is given in Table 1.

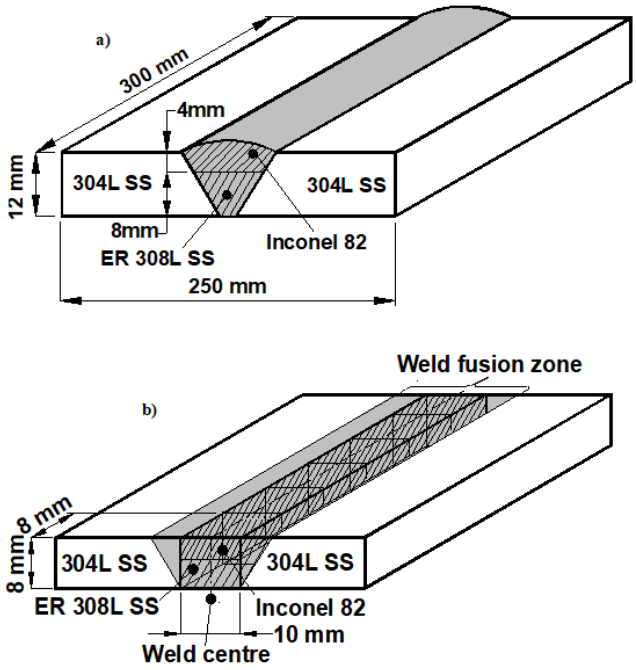


**Figure 1.** (a) 304L SS weld pad fabricated by joining two 304L SS plates using 308L SS filler wire (8 mm deposit) and Inconle 82 filler wire (4 mm deposit over 308L SS); (b) depicts 10 mm (wide) × 300 mm (length) × 8 mm (height) sectioned out from the fusion zone of the weld pad and further 10 mm (wide) × 8 mm (height) × 8 mm (length) specimens incised from the weld fusion zone

For the fabrication of Inconel 82 weld overlay on 304L SS weld metal, two 12 mm thick 304L SS base plates were joined by multipass gas tungsten arc welding (GTAW) process in accordance with ASME section IX of boiler and pressure vessel code.[23] The 8 mm of 308L SS filler wire was initially deposited, above which, 4 mm of Inconel 82 filler wire was deposited, as shown in Figure 1a. The welding parameters for the root pass weld are current = 67 A, arc voltage = 10 V; welding speed = 32 mm/ min and that for the remaining weld passes are current = 95 A, arc voltage = 11 V; welding Speed = 75 mm / min and the inter pass temperature : $< 120$ °C.

The weld pad was qualified by radiography. 1 mm from the top surface and 3 mm from the root side of the weld zone was machined out. Subsequently, 5 mm on either side of the weld central line was marked and sectioned out of the weld pad to obtain 10 mm (wide) x 300 mm (length) x 8 mm (height) of the weld fusion zone (Figure 1b). From this fusion zone, specimens of dimension 10 mm wide x 8 mm length x 8 mm height (Figure 1b) were further cut out by electrical discharge machining (EDM) and used for EN investigation in 0.01 M $FeCl_3$. For convenience, the Inconel 82 weld overlay on 304L SS weld metal will be referred to as Inconel 82 weld overlay in the forthcoming sections of the manuscript.

**Table 1.** Chemical Composition of 304L SS base, 308L SS filler wire and Inconel 82 filler wire used for the fabrication of the Inconel 82 weld overlay on 304L SS weld

| Material | C | Mn | Cr | Mo | Fe | Nb/Ta | Cu | Ti | Si | P | S | Ni |
|---|---|---|---|---|---|---|---|---|---|---|---|---|
| 304L SS | 0.025 | 1.66 | 18.11 | 0.4 | balance | - | - | - | 0.41 | 0.03 | 0.02 | 9 |
| 308L SS | 0.022 | 1.71 | 19.62 | 0.041 | balance | - | 0.084 | - | 0.36 | 0.021 | 0.005 | 9.16 |
| Inconel 82 filler wire | 0.03 | 2.85 | 20.4 | - | 1.1 | 2.5 | - | | 0.22 | 0.003 | 0.001 | 72.9 |

## 2.1 Optical microscopy

Inconel 82 weld overlay specimen was mechanically ground till 1000 grit emery sheet and further polished till diamond finish. Electrolytic etching of the polished surface was carried out in 10% oxalic acid for 5 s at 6 V. The etched surface was observed under an optical microscope.

## 2.2 Electrochemical Noise Measurement

Three nominally identical electrodes made of Inconle 82 weld overlay were mounted in an alardite hardener resin and ground mechanically using silicon carbide emery sheets and polished up to a diamond mirror finish. The mounted specimens were immersed in 0.01 M $FeCl_3$, so that an area of 0.8 $cm^2$ of the top surface of the weld overlay was exposed. Two of such identical electrodes coupled through a zero resistance ammeter served as the working electrodes (1 and 2) and the third identical electrode was made the reference electrode. Since the reference electrode is also identical to the working electrode, it is referred to as the pseudo-reference electrode.[18,20,21] The EN cell was placed inside a Faraday cage for minimising external noise. Potential noise measurements were made between the coupled working electrodes and the pseudo-reference electrode, using a multichannel electrochemical noise system, Autolab PGSTAT 30 (Ecochemie make, The Netherlands). Measurements were made under freely corroding conditions at a sampling interval of 0.5 s for 5 h of immersion. The frequency domain corresponding to the sampling conditions was evaluated using $f_{max}$ = 1/2t and $f_{min}$ = 1/Nt, where, t is the sampling interval and N is the total number of data points. For $\Delta$t = 0.5 s and N = 8192, the frequency domain was evaluated to be between 1 Hz ($f_{max}$) and 0.2 mHz ($f_{min}$). These experimental details have been elaborated in our earlier reports.[24–26] As the reference electrode used is identical to the coupled working electrodes, and hence called the pseudo-reference electrode, there would be two sources contributing to the potential noise signal. If the potential noise from the coupled working electrodes is designated as $E_1$, and that from the pseudo-reference electrode is $E_2$, the measured potential noise ($E_m$) can be represented as

$$E_m = \sqrt{(E_1^2 + E_2^2)} \quad (1)$$

Since the electrodes are identical, it is assumed that the contributions $E_1$ and $E_2$are equivalent and hence, the potential noise for the working electrode can be obtained by a simple mathematic rearrangement of Equation (1).[27–29] The potential noise data obtained after correcting the contribution from the pseudo-reference electrode was used for the analysis.

## 2.3 Antialiasing

Aliasing of EN signal occurs when the digital time record contains low frequency components that are absent in the analog signal, due to the presence of high frequency components in the analog signal. An aliased EN signal will appear in the power spectral plots as a flattening of the high frequency end. To avoid aliasing, the analog signal should not contain frequency components greater than the Nyquist frequency and hence these frequencies have to be eliminated before analog to digital (A/D) conversion, which could be achieved by using low pass filters.[20,30,31] As these filters are high-priced, filtering based on digital processing has been employed by some manufacturers of EN systems.[30] One method that is reported in literature[30] explains that the data sampling is done at a fixed high frequency ($f_h$) and a low pass filter is used at a fixed cut off frequency. Subsequently, the average over n points is retained, where, n = ($f_h$/$f_s$), and $f_s$ denotes the desired sampling frequency. For eliminating signal aliasing, Autolab PGSTAT 30 has a low pass filter (with a cut off of 1 KHz) incorporated at the input stage. The ADC module then samples the signals at the highest sampling rate, of the order of 50 kHz, and the A/D values obtained are averaged over the desired sampling interval and provided in the data.

# 3 Data Analysis

## 3.1 Data treatment

The acquired EN signal contains noise amplitudes that are superimposed on a direct current (DC) drift or trend,

which is not useful to explain the corrosion phenomenon and hence has to be removed. The DC trend refers to the variation of the mean current or potential divided by time. Assuming that the trend varies linearly over a small time interval, a linear fit method[26,32–34] was used to remove the trend and obtain the pure noise amplitude, which was used for analysis.

## 3.2 Wavelet Analysis

Statistical and spectral methods that are popularly used to analyze EN signals are formulated for stationary signals (statistical properties do not change with time), as these methods average the information across the entire EN-time record. Wavelet transform has been devised to study stationary and non-stationary signals as well.[35,36] As EN signals are by and large non-stationary, the wavelet transforms serve as a valuable tool to obtain useful information from corrosion processes generating the EN signals. Wavelet analysis uses transients with a finite duration known as wavelets, and these have an average value of zero.[35–39] An advantage of wavelet analysis is that the time domain information is preserved and non-stationary time records can be analyzed without detrending and windowing.[40]

In the present investigation, the orthogonal wavelet transform, (OWT), was used to analyze the detrended potential noise-time record.[38,39] In this method, as well reported in literature,[35–40] an EN time record, x(t) = $X_n$ (n = 1....N) is represented as a linear combination of basis functions $\Phi_{j,k}$ and $\psi_{j,k}$

$$x(t) = \sum_k s_{j,k}\varphi_{j,k}(t) + \sum_k d_{j,k}\psi_{j,k}(t) + \sum_k d_{j-1,k}\psi_{j-1,k}(t) + \ldots + \sum_k d_{1,k}\psi_{1,k}(t) \quad (2)$$

Where, $\phi_{j,k}(t) = 2^{-j/2}\psi\,(2^{-j}t - k)$ and $\varphi_{j,k}(t) = 2^{-j/2}\varphi((2^{-j}t - k)$, *j, k* $\epsilon$ *Z* where Z is a set of integers and *k = 1,2 ... N/2,* N is the number of data record, j = 1,2,...j and j is a small natural number that depends on N, $s_{j,k}$,$d_{j,k}$, ....$d_{1,k}$ is referred to as the smooth coefficient and the detailed coefficients respectively.

In wavelet analysis, the EN signal is passed through a series of high and low pass filters to obtain detailed and smoothed coefficients. At the commencement, the low frequencies of the signal pass through a low pass filter, and high frequencies pass through a high pass filter, producing the set of smooth coefficients, S1($s_{1,1}$, $s_{1,2}...s_{1,N/2}$) and detailed coefficients, D1($d_{1,1}$, $d_{1,2}...d_{1,N/2}$). The set of detailed coefficients called as crystals or partial signal is kept aside for analysis, and the smooth coefficients (S1) is further filtered in the next stage to produce $S_2$ and $D_2$. A schematic representation of a two level decomposition of the EN signal is shown in Figure 2.

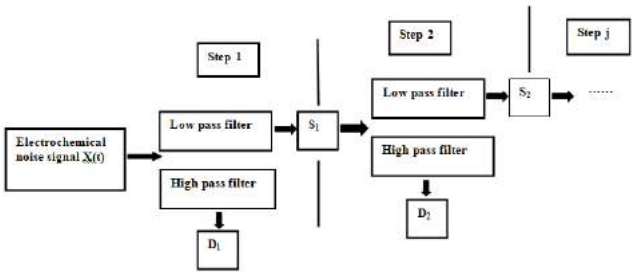


**Figure 2.** General scheme of the orthogonal wavelet transform

The scale range[41,42] of each crystal is given by $(2^{-j}t, 2^{j-1}t)$ where t represents the sampling interval.

In the present study, an eight level decomposition was used ( j = 8), and hence this process was iterated successively eight times to decompose the signal into $D_1$, $D_2$....D8 and S8 set of coefficients. The crystals, D1...D8, resemble the fluctuations of the acquired EN signal at a particular interval of frequency. The property of the OWT is that the sum of the relative energies of these crystals will give the energy of the EN signal.

$$\mathrm{E} = \mathrm{E_{D1}} + \mathrm{E_{D2}} + \mathrm{E_{D3}} + \mathrm{E_{D4}} + \mathrm{E_{D5}} + \mathrm{E_{D6}} + \mathrm{E_D}7 + \mathrm{E_{D8}} + \mathrm{S_8} \quad (3)$$

Where Eisthe energy of the EN signal containing N data points given by

$$E = \sum_{n=1}^{N} x_n^2 \quad (4)$$

$E_{D1}$, $E_{D2}$, $E_{D3}$, $E_{D4}$, $E_{D5}$, $E_{D6}$, $E_{D7}$, $E_{D8}$ and $E_{S8}$are the relative energies given by

$$E_j^d = \frac{1}{E}\sum_{n=1}^{N} d_{j,n}^2 \quad \text{and} \quad E_j^s = \frac{1}{E}\sum_{n=1}^{N} s_{j,n}^2 \quad (5)$$

Where $E_j^d$ and $E_j^s$ are the relative energies of the detailed coefficients and smoothed coefficients respectively. As $S_8$ represents the trend of the signal, it is not used for analysis. The relative energies of the crystals can be plotted against the name of the crystals (D1...D8) to give energy distribution plots (EDP), which represents the relative contribution of every crystal to the EN signal and are useful to derive mechanistic information about the type of processes occurring on the material surface. In the present investigation, the decomposition of the signal was carried out using orthogonal Daubechies wavelet of the fourth order (db4). It is reported[42] that among the various families of wavelets, the Daubechies 4 or "db4"

is highly localized in time and is useful for EN studies.

## 4 Results and Discussion

### 4.1 Microstructural investigation

Figure 3 shows the optical micrograph of Inconel 82 weld overlay that depicts a fully austenitic microstructure containing equiaxed dendrites or subgrains. The boundary separating the subgrains called the solidification sub grain boundaries (SSGB) is indicated by arrows in the micrograph. The SSGB are low angle boundaries that result from the growth of sub grains along preferred crystallographic direction.[43] The microstructure shows secondary precipitates at the interdendritic regions along the SSGB. Similar observations have been reported by Lee *et al*.[44] These secondary phases have been reported to be Nb-rich carbides (NbC), and intermetallic Laves phase.[43,45–47] The Laves phases are brittle intermetallic compounds that have an $AB_2$ stoichiometry. In general, the composition of Laves phase in Nb bearing Ni-based superalloys has been reported to be (Ni, Fe, Cr)$_2$Nb, which are rich in Nb, and lean in Ni, Fe and Cr [43, 47]. In Nb bearing Ni base superalloys, the solidification terminates by a eutectic reaction between the $\gamma$ phase and Nb-rich phases, such as NbC and the Laves phase. The literature reports that the solidification proceeds through the primary crystallization of austenite phase ($\gamma$) with the dendritic cores getting more enriched in the alloying elements, Fe, Cr, Ni, as the solidification proceeds, and minor elements such as Nb getting segregated at the interdendritic region, where they precipitate as Nb - rich phases towards the terminal stage of solidification.[45,46] Microsegregation of Nb to the liquid phase in the interdendritic region and subsequent formation of Nb-rich phases during solidification of Ni-based superalloys is well documented in the literature [43, 47]. Figure 4a depicts the SEM image of Inconel 82 weld overlay and Figure 4b is the magnified SEM image showing the precipitates in the interdendritic region along the SSGB. The white precipitates in the SEM image are the secondary phases. The energy dispersive x-ray spectra of the matrix and the precipitates taken in the SEM-EDS mode are shown in Figure 5a & 5b, and the elemental analysis of the same is given alongside. The matrix is enriched in Fe, Cr, and Ni, and is lean in Nb, while the precipitate is enriched in Nb, and slightly depleted of Fe, Cr and Ni. Hence, these white precipitates are the Laves phases of type (Ni, Fe, Cr)$_2$Nb.

### 4.2 EN-time record and energy distribution plots from wavelet analysis

The EN-time records present the spontaneous random potential or current fluctuations acquired with respect

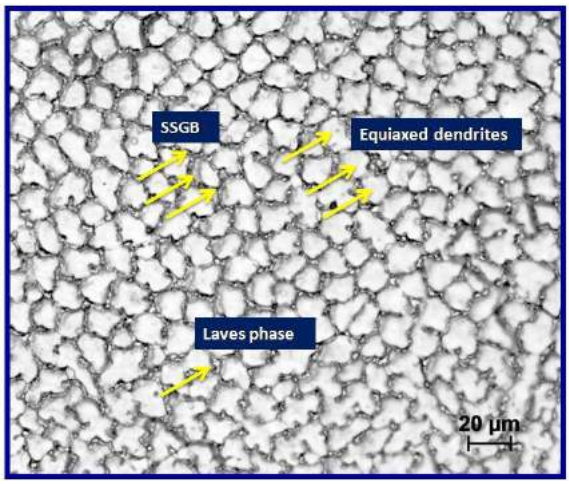


**Figure 3.** Microstructure of Inconel 82 weld overlay depicting dendritic structure with precipitates at the interdendritic region

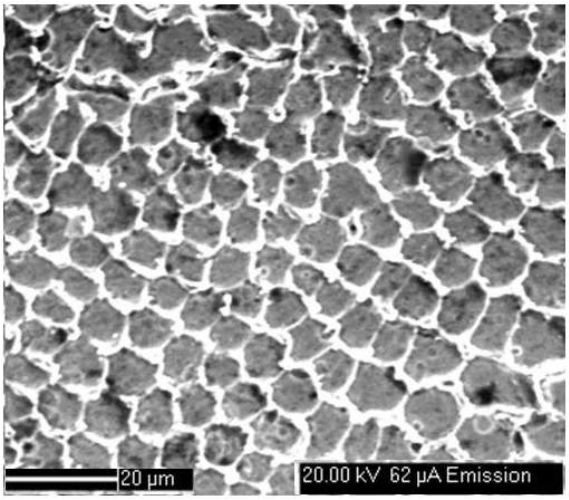


(a)

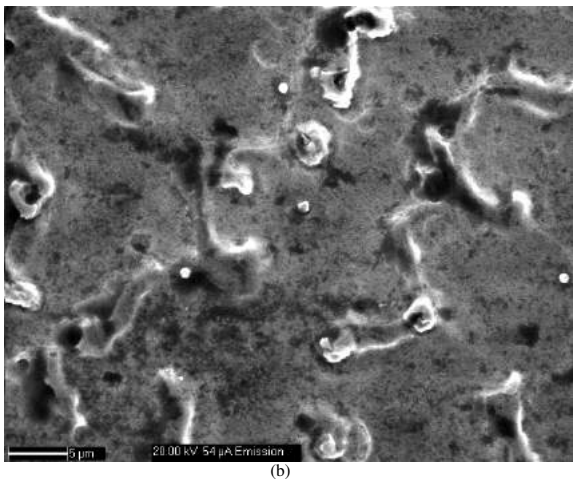


(b)

**Figure 4.** (a) SEM of Inconel 82 weld overlay depicting dendritic structure with precipitates at the interdendritic region; (b) magnified SEM image showing the Laves phase as white precipitates, along the interdendritic region

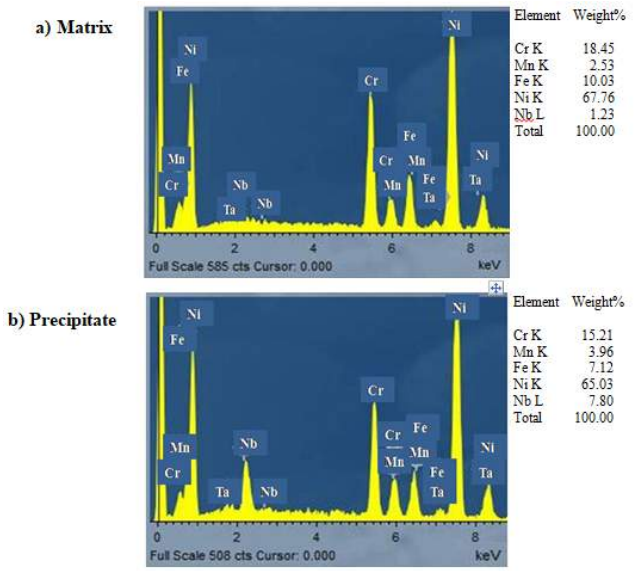


**Figure 5.** SEM-EDS of Inconel 82 weld overlay with the elemental analysis given along side, a) matrix b) precipitate showing Nb enrichment

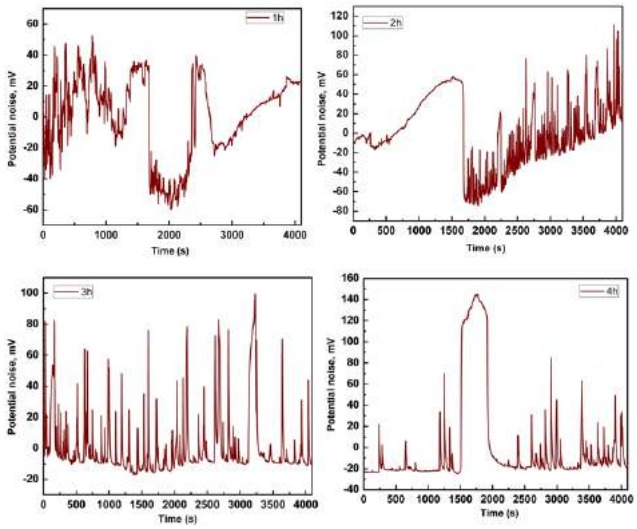


**Figure 6.** Trend removed electrochemical potential noise time record taken after a) 1 h, b) 2 h, c) 3 h, d) 4 h of immersion

to time and it is an accepted method to visually examine the fluctuations as the first step of the data analysis.[20,21] EN-time record can be interpreted by analyzing the shape, size and distributions of potential or current transients measured during the corrosion processes. It is a well recognized fact that the potential noise-time record or current noise-time record depicts discrete features for various types of corrosion, be it uniform or localized (pitting, crevice, intergranular corrosion, and stress corrosion cracking (SCC)).[21,24–26,31,48–53] Nevertheless, the EN-time records cannot be considered as conclusive evidence of the processes, and hence the acquired EN-time records should be further analyzed in the time domain by employing statistical methods or in the frequency domain. Alternatively, other analysis methods like shot noise, wavelet transforms, *etc*. [20, 21] can be used. It is essential to remove the trend in the EN - signals and present the noise data in simple noise amplitudes. The trend removed electrochemical potential noise-time record during immersion of Inconel 82 in 0.01 M $FeCl_3$ is represented in Figure 6. The time record after 1 h of immersion showed random fluctuations, and after 2 h of immersion, high amplitude potential transients in the range of 20-80 mV appeared in the time record. After 3 h and 4 h of immersion, the potential transients became more distinct, with the amplitude increasing to 80-120 mV range. These distinct high amplitude noise transients are typical during the localized attack.[20,21,29]

The EDP from wavelet analysis has been widely used in corrosion research to monitor the processes occurring on a material surface and distinguish various types of corrosion.[35–39,54–57] For instance, Wang *et al*.[54] have reported that the EDP from potential noise measurements for general and passivation process have the maximum relative energy concentrated on D1 crystals, while that for pitting and crack propagation show maximum energy on the D7 crystal. Also, the potential noise EDP for intergranular corrosion showed maximum energy on D7 and D1 as well. In a study made earlier on pitting of 304L SS in ferric chloride medium, the EDP indicated maximum energy distribution on D6-D8 crystals.[55] Smith *et al*.[56] have used wavelet analysis to distinguish between general and pitting corrosion of ASTM A516 steel in sodium hydroxide medium with and without chloride additions. The authors reported that the maximum relative energy was defined on the large time scale crystals during pitting attack. According to literature reports,[38,39,57] the position of the maximum relative energy of a crystal determines the predominant process that is contributing to the EN signal and relates to the process occurring on the material surface. For an eight level decomposition or for j = 8, the time scale of the crystals increases in the order D1 $<$ D2 $<$ D3 $<$ D4 $<$ D5 $<$ D6 $<$ D7 $<$ D8 (as shown in Table 2). The EDP for an eight level decomposition can be classified into three regions. If the maximum relative energy is defined on smaller time scale crystals, D1-D3, it implies that rapid events such as metastable pitting are occurring on the material surface. Maximum relative energy on medium time scale crystals, D3-D6, indicates processes such as repassivation / propagation of pits. The third region comprises large time scale D6-D8 crystal and the energy defined on these crystals implies that slow pro-

cesses such as diffusion or growth of pits are predominant.[58–61] Also, the values of the energies of the crystals or partial signal in the EDP plot indicate the domination of that particular crystal or partial signal in the original acquired EN-time record. Higher the value of the energy of the crystal, greater is the contribution of the partial signal to the acquired EN-time record.

**Table 2.** Scale range for j=8, t = 0.5 s

| Crystal name | D1 | D2 | D3 | D4 | D5 | D6 | D7 | D8 |
|---|---|---|---|---|---|---|---|---|
| Scale range(s) | 0.5-1 | 1-2 | 2-4 | 4-8 | 8-16 | 16-32 | 32-64 | 64-128 |

The EDP plots for Inconel 82 in 0.01 M $FeCl_3$after 1 h, 2 h, 3 h, and 4 h are presented in Figure 7. The EDP after 1 h of immersion indicates maximum relative energy on crystals D6-D8, which implies that crystals, D6-D8, dominate the originally acquired noise - time record. These are large time scale crystals corresponding to localized events. Some relative energy is also defined on D4 and D5 crystals, which are medium time scale crystals depicting processes like repassivation events. The observation indicates that the predominant process occurring on the material surface is a localized attack and that apart, some repassivation events pertaining to film breakdown and repair are also prevailing. The lower values of the relative energy indicate that frequency of occurrence of the localized events is low. This is in agreement with the potential noise time record taken after 1 h of immersion that shows few distinct potential transients combined with random signals.

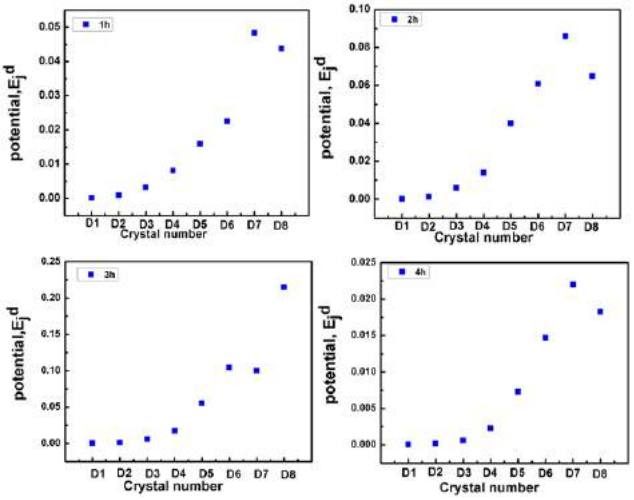


**Figure 7.** Energy distribution plots (EDP) of potential noise from wavelet analysis for Inconel 82 weld overlay in 0.01 M $FeCl_3$

Similarly, the EDP plots after 2 h, 3 h, and 4 h of immersion also depict maximum relative energy on D6-D8,

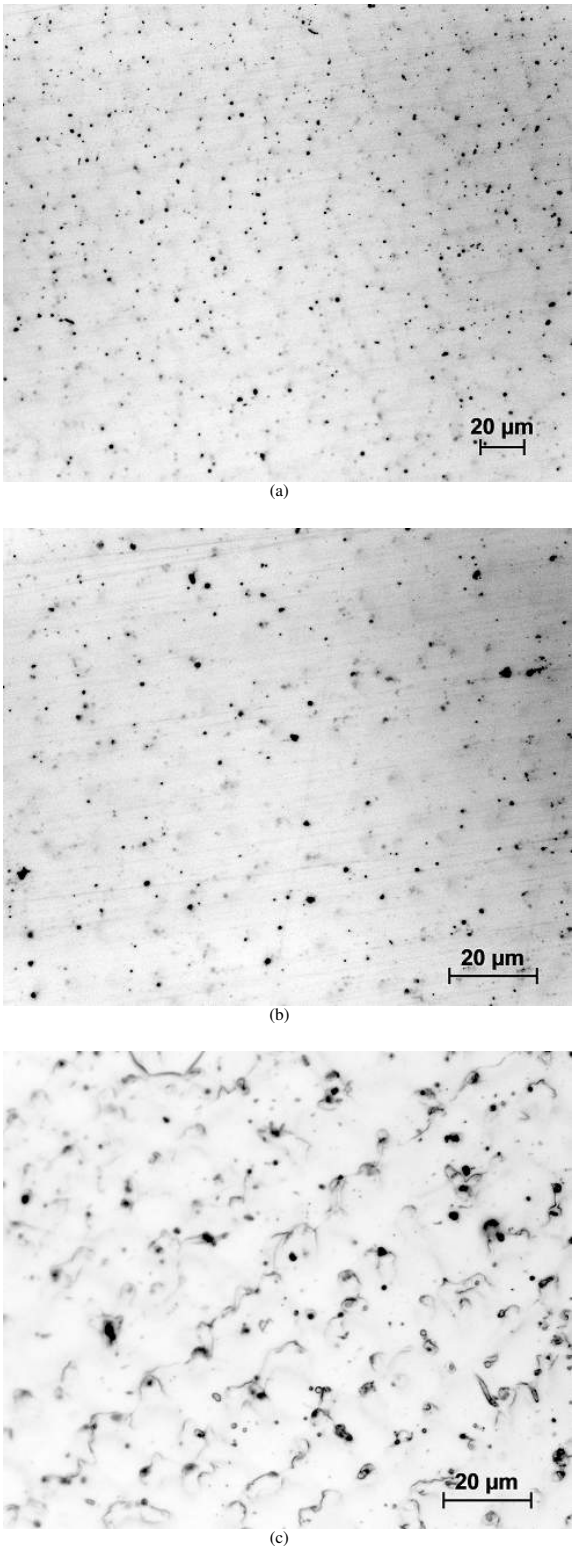


**Figure 8.** Optical micrograph of the Inconel 82 weld overlay after, (a & b) EN experiment in 0.01 M $FeCl_3$ showing localized attack at the interdendritic region, at two different locations of the specimen; (c) EN experimented specimen after mild etching in oxalic acid confirming that the localized attack are at the interdendritic region. The dendrites are free of localized attack.

with the maximum on D7 and D8 and some energy defined on D4 and D5. The position of the relative energy in the EDP after 2 h, 3 h, and 4 h specify that the prevailing corrosion mechanism is a localized dissolution. It is further observed that there is a progressive increase in relative energy values after 2 h and 3 h of immersion, which is an implication of an increase in the occurrence of the localized attacks. The potential noise time record too shows an increase in the distinct potential transients after 2 h and 3 h of immersion. The relative energy after 4 h of immersion has again decreased indicating that the frequency of occurrence of the attacks has decreased at that instant, which is in agreement with the time record that also shows a decrease in the number of distinct transients after 4 h of immersion when compared with that after 3 h of immersion. Thus, it could be concluded that the predominant process occurring on the material surface is related to the localized attack, with some repassivation processes also occurring in tandem, but to a lower extent and the frequency of occurrence of the localized attack is variable at different times. A good correlation is obtained between the results from the EDP and the potential noise time record. The optical micrograph after the EN experiment (at two different locations of the specimen) that was carried out for 5h of immersion in 0.01 M $FeCl_3$ is shown in Figure 8a & 8b. The micrograph reveals localized attacks at the interdendritic region along the SSGB and no attack within the dendrites. The appearance of SSGB indicates that the specimen has undergone mild etching. Nevertheless, the extent is much less as a result of which the appearance is very feeble. The localized attacks could be attributed to the presence of a continuous network of Nb-rich secondary phases at the interdendritic region, where, the passive film formed would be weak, and chloride ions can easily adhere, penetrate and cause localized break down of the film, leading to localized dissolution in the vicinity of the secondary phases. The micrographs show attacks only in the interdendritic region along the SSGB. To confirm the same, the experimented specimen was etched mildly with oxalic acid, and the optical micrograph was taken (Figure 8c). It is evident that the dendrites are free of any attack and the attacks are confined to localized areas along the interdendritic region. The high resistance of the matrix to localized attack could be attributed to the passive film stability rendered by high chromium content of the alloy as well as to the presence of Nb. It is reported that Nb as a minor alloying element present in the austenite matrix of Ni-based superalloys enhances the passive film stability and thus resist corrosion attack. A good correlation exists between the post-experimental micrographs and the results from the potential noise time record that indicates the mode of attack to be localized.

The potential transients observed in the EN-time records are thus pertaining to the localized dissolution at the interdendritic region, and hence it could be inferred that the presence of Nb-rich secondary phases in Inconel 82 weld overlay has been detrimental to the localized corrosion resistance. This result is also in good agreement with the results from EDP plots that depict localized events as the predominant process. EDP has been found to be useful in deducing the corrosion mechanism.

## 5 Conclusion

Inconel 82 weld overlay on 304L SS weld metal fabricated by multipass GTAW process revealed a full austenite microstructure, containing equiaxed dendrites and Nb-rich secondary phases along the interdendritic region. The secondary phases were identified to be the Laves phase, [$(Ni, Cr, Fe)_2$ Nb] from SEM-EDS analysis. Electrochemical potential noise monitoring of Inconel 82 weld overlay on 304L SS weld in 0.01 M $FeCl_3$ medium revealed distinct high amplitude potential transients, typical of localized attack. The EDP derived from wavelet analysis of the potential noise time records indicated localized attack to be the predominant process throughout monitoring, with variable frequency of occurrence. Also, repassivation events could be demarcated from the EDP. A variation in the relative energy value indicated that the frequency of occurrence of localized attack varied at different times of immersion. The localized attack was confirmed to be along the interdendritic region as a consequence of the presence of Nb-rich secondary phases. The equiaxed dendrites were found to be free of localized attack, which could be attributed to the high chromium content of the alloy and the presence of minor alloying element Nb, which is known to enhance the passive film stability. A good correlation was obtained between the results of the EDP and the potential noise time record, both of which depicted the progress of corrosion. The EDP from EN analysis has been found to be a useful tool to monitor the progress on localized corrosion of Inconel 82 weld overlay in 0.01M $FeCl_3$. The study indicated that the presence of Laves phase along the SSGB decreased the localized corrosion resistance of the weld overlay. Thus, optimizing the welding parameters or adopting advanced welding methods to reduce the formation of the secondary phases is beneficial to enhance the localized corrosion resistance of the weld overlay.

## References

[1] Introduction to Stainless Steels, ASM International, J.R.Davis, Davis & Associates, 1994, p110.

[2] Matsui M, Komai N, Miyazawa T, *et al*. Corrosion Characteristics and Mechanical Properties of Inconel 622 Weld Overlay of Waterwall Tubes in Coal Fired Boilers. Quarterly Journal of Japan Welding Society, 2009, **27**(2): 149-153. https://doi.org/10.2207/qjjws.27.149s

[3] Paul L, Eckhardt M, Clark G, *et al*. Experience with Weld Overlay and Solid Alloy Tubing Materials in Waste to Energy Plants, 12th North American Waste to Energy Conference May 17-19,Savannah, Georgia USA NAWTEC12-2216, 2004. https://doi.org/10.1115/NAWTEC12-2216

[4] Craig BD and Smith L. Corrosion Resistant Alloys (CRAs) in the Oil and Gas Industry, Nickel Institute Technical Series No.1 0073, September 2011, p 1-10.

[5] Celin R and Tehovnik F. Degradation of a Ni-Cr-Fe Alloy in a Pressurised-Water Nuclear Power Plant. Materials Technology, 2011, **45**(2): 151-157.

[6] Riccardella PC, Hirschberg P, Anderson T, *et al*. The Role of Displacement-Controlled Stresses in Critical Flaw Size Determination for Piping Systems. ASME. Pressure Vessels and Piping Conference. Materials and Fabrication, Parts A and B, 2008, **6**:1087-1092. https://doi.org/10.1115/PVP2008-61074

[7] Bhaduri AK, Venkadesan S, Rodriguez P, *et al*. Transition Metal Joints for Steam Generators-An Overview, International Journal of Pressure Vessels and Piping, 1994, **58**(3) 251-265. https://doi.org/10.1016/0308-0161(94)90061-2

[8] Persaud SY, Ramamurthy S, Newman RC. The effect of weld chemistry on the oxidation of Alloy 82 dissimilar metal welds. Corrosion Science, 2015, **91**: 58-67. https://doi.org/10.1016/j.corsci.2014.10.044

[9] Rathod D, Aravindan S, Singh PK, *et al*. Metallurgical Characterization and Diffusion Studies of Successively Buttered Deposit of Ni-Fe Alloy and Inconel on SA508 Ferritic Steel. ISIJ International, 2014, **54**(8): 1866-1875. https://doi.org/10.2355/isijinternational.54.1866

[10] Lee HT and Kuo TY. Analysis of microstructure and mechanical properties in alloy 690 weldments using filler metals I-82 and I-52. Science and Technology of Welding and Joining, 1999, **4**(2): 94-103. https://doi.org/10.1179/136217199101537626

[11] Hu JN, Fukahori T, Igari T, *et al*. An evaluation of creep rupture strength of ferritic/austenitic dissimilar weld interfaces using cohesive zone modelling. Procedia Structural Integrity, 2016, **2**: 934-941. https://doi.org/10.1016/j.prostr.2016.06.120

[12] Mortezaie A, Shamanian M. An assessment of microstructure, mechanical properties and corrosion resistance of dissimilar welds between Inconel 718 and 310S austenitic stainless steel. International Journal of Pressure Vessels & Piping, 2014, **116**(1): 37-46. https://doi.org/10.1016/j.ijpvp.2014.01.002

[13] Briant CL and Hall EL. The microstructural causes of intergranular corrosion of Alloys 82 and 182. Corrosion, 1987, **43**(9): 539-548. https://doi.org/10.5006/1.3583898

[14] H anninen H, Aaltonen P, Brederholm A, *et al*. Dissimilar metal weld joints and their performance in nuclear power plant and oil refinery conditions. VTT research notes, 2006, 2347. https://doi.org/10.13140/RG.2.1.3104.5608

[15] Page RA and McMinn A. Relative stress corrosion susceptibilities of alloys 690 and 600 in simulated boiling water reactor environments. Metallurgical Transactions A, 1986, **17**(5): 877-887. https://doi.org/10.1007/BF02643864

[16] Kamachi M, Dayal RK and Gnanamoorthy JB. Corrosion studies on materials of construction for spent nuclear fuel reprocessing plant equipment. Journal of nuclear materials, 1993, **203**(1): 73-82. https://doi.org/10.1016/0022-3115(93)90432-X

[17] Suresh G, Dasgupta A, Kishor P, *et al*. Effect of laser surface melting on the microstructure and pitting corrosion resistance of 304L SS weldment. Metallurgical and Materials Transactions B, 2017, **48**(5): 2516-2525. https://doi.org/10.1007/s11665-016-2488-3

[18] Electrochemical noise measurement for corrosion applications. ASTM International, 1996. https://doi.org/10.1520/STP1277-EB

[19] Cottis RA. Interpretation of electrochemical noise data. Corrosion, 2001, **57**(3): 265-285. https://doi.org/10.5006/1.3290350

[20] Giriga S, Mudali UK, Raju VR, *et al*. Electrochemical noise technique for corrosion assessment-a review[J]. Corrosion Reviews, 2005, **23**(2-3): 107-170. https://doi.org/10.1515/CORRREV.2005.23.2-3.107

[21] Girija S, Nandakumar T and Mudali U K. Corrosion Behavior of Alloy 625 in Simulated Nuclear High-Level Waste Medium. Journal of Materials Engineering and Performance, 2015, **24**(11): 4421-4430. https://doi.org/10.1007/s11665-015-1714-8

[22] Girija S and Kamachi Mudali U. Electrochemical noise resistance evaluation of 304L SS in nitric acid and simulated nuclear high level waste. Corrosion Engineering, Science and Technology, 2014, **49**(5): 335-344. https://doi.org/10.1179/1743278213Y.0000000137

[23] Girija S, Mudali UK, Khatak HS, *et al*. The application of electrochemical noise resistance to evaluate the corrosion resistance of AISI type 304 SS in nitric acid. corrosion science, 2007, **49**(11): 4051-4068. https://doi.org/10.1016/j.corsci.2007.04.007

[24] Suresh G, Mudali UK and Raj B. Corrosion monitoring of type 304L stainless steel in nuclear near-high level waste by electrochemical noise. Journal of Applied Electrochemistry, 2011, **41**(8): 973-981. https://doi.org/10.1007/s10800-011-0324-x

[25] Dawson JL. Electrochemical noise measurement: the definitive in-situ technique for corrosion applications? Electrochemical noise measurement for corrosion applications. ASTM International, 1996. https://doi.org/10.1520/STP37949S

[26] Reichert DL. Electrochemical Noise Measurements for Determining Corrosion Rates, in: Electrochemical Noise Measurements for Corrosion Applications. ASTM Philadelphia, 1996.

[27] Girija S, Mudali UK, Raju VR, *et al*. Determination of corrosion types for AISI type 304L stainless steel using electrochemical noise method. Materials Science and Engineering: A, 2005, **407**(1-2): 188-195. https://doi.org/10.1016/j.msea.2005.07.022

[28] Bastos IN, Huet F, Nogueira RP, *et al*. Influence of aliasing in time and frequency electrochemical noise measurements. Journal of the Electrochemical Society, 2000, **147**(2): 671-677.
https://doi.org/10.1149/1.1393251

[29] Bosch RW, Cottis RA, Csecs K, *et al*. Reliability of electrochemical noise measurements: Results of round-robin testing on electrochemical noise. Electrochimica Acta, 2014, **120**: 379-389.
https://doi.org/10.1016/j.electacta.2013.12.093

[30] Bertocci U, Huet F, Nogueira RP, *et al*. Drift removal procedures in the analysis of electrochemical noise. Corrosion, 2002, **58**(4): 337-347.
https://doi.org/10.5006/1.3287684

[31] Al-Mazeedi HAA, Cottis RA. A practical evaluation of electrochemical noise parameters as indicators of corrosion type. Electrochimica Acta, 2004, **49**(17-18): 2787-2793.
https://doi.org/10.1016/j.electacta.2004.01.040

[32] Mansfeld F, Sun Z, Hsu CH, *et al*. Concerning trend removal in electrochemical noise measurements. Corrosion Science, 2001, **43**(2): 341-352.
https://doi.org/10.1016/S0010-938X(00)00064-0

[33] Wharton JA, Wood RJK and Mellor BG. Wavelet analysis of electrochemical noise measurements during corrosion of austenitic and superduplex stainless steels in chloride media. Corrosion science, 2003, **45**(1): 97-122.
https://doi.org/10.1016/S0010-938X(02)00140-3

[34] Aballe A, Bethencourt M, Botana F J, *et al*. Use of wavelets to study electrochemical noise transients. Electrochimica Acta, 2001, **46**(15): 2353-2361.
https://doi.org/10.1016/S0013-4686(01)00424-8

[35] Shahidi M, Hosseini SMA and Jafari A H. Comparison between ED and SDPS plots as the results of wavelet transform for analyzing electrochemical noise data. Electrochimica Acta, 2011, **56**(27): 9986-9997.
https://doi.org/10.1016/j.electacta.2011.08.091

[36] Aballe A, Bethencourt M, Botana F J, *et al*. Wavelet transform-based analysis for electrochemical noise. Electrochemistry communications, 1999, **1**(7): 266-270.
https://doi.org/10.1016/S1388-2481(99)00053-3

[37] Aballe A, Bethencourt M, Botana F J, *et al*. Using wavelets transform in the analysis of electrochemical noise data. Electrochimica Acta, 1999, **44**(26): 4805-4816.
https://doi.org/10.1016/S0013-4686(99)00222-4

[38] Malamud BD and Turcotte DL. Self-affine time series: measures of weak and strong persistence. Journal of statistical planning and inference, 1999, **80**(1-2): 173-196.
https://doi.org/10.1016/S0378-3758(98)00249-3

[39] Mohsenifar F and Jafari AH. Comparison of Energy of Wavelet Coefficients as a Useful Tool for Interpreting of EN Data. App Math in Eng Manag Tech, 2015, **3**(1): 794 -804.

[40] Smith MT and Macdonald DD. Wavelet Analysis of Electrochemical Noise Data. Corrosion, 2009, **65**(7): 438-448.
https://doi.org/10.5006/1.3319148

[41] Lippold JC, Kiser SD and DuPont JN. Welding Metallurgy and weldability of Nickel base alloys, Microstructural Evolution in the Fusion Zone, p57.

[42] Lee J, Jang CH, Kim JS, *et al*. Mechanical Properties Evaluation in Inconel 82/182 Dissimilar Metal Welds. Transactions of SMiRT, 2007, 19.

[43] Sireesha M, Albert SK, Shankar V, *et al*. A comparative evaluation of welding consumables for dissimilar welds between 316LN austenitic stainless steel and Alloy 800. Journal of Nuclear Materials, 2000, **279**(1): 65-76.
https://doi.org/10.1023/A:1017308021429

[44] Naffakh H, Shamanian M and Ashrafizadeh F. Dissimilar welding of AISI 310 austenitic stainless steel to nickel-based alloy Inconel 657. Journal of materials processing technology, 2009, **209**(7): 3628-3639.
https://doi.org/10.1016/j.jmatprotec.2008.08.019

[45] DuPont JN and Robino CV. The influence of Nb and C on the solidification microstructures of Fe-Ni-Cr alloys. Scripta materialia, 1999, **41**(4): 449-454.
https://doi.org/10.1016/S1359-6462(99)00102-5

[46] Terry MT, Edgemon GL, Mickalonis J I, *et al*. Development and deployment of advanced corrosion monitoring systems for high-level waste tanks. Los Alamos National Laboratory PO Box 1663, Los Alamos, NM (US); HiLine Engineering and Fabrication 2105 Aviator Dr., Richland, WA; Westinghouse Savannah River Company Savannah River Technology Center, Aiken, SC; Idaho National Engineering and Environmental Laboratory PO Box 1625, Idaho Falls, ID (US), 2002.

[47] Roberge PR, Beaudoin R and Sastri VS. Electrochemical noise measurements for field applications. Corrosion science, 1989, **29**(10): 1231-1233.
https://doi.org/10.1016/0010-938X(89)90069-3

[48] Hladky K and Dawson JL. The measurement of localized corrosion using electrochemical noise. Corrosion Science, 1981, **21**(4): 317-322.
https://doi.org/10.1016/0010-938X(81)90006-8

[49] Samantaroy PK, Suresh G, Paul R, *et al*. Corrosion behavior of Alloy 690 and Alloy 693 in simulated nuclear high level waste medium. Journal of Nuclear Materials, 2011, **418**(1-3): 27-37.
https://doi.org/10.1016/j.jnucmat.2011.07.005

[50] Gabrielli C and Keddam M. Review of applications of impedance and noise analysis to uniform and localized corrosion. Corrosion, 1992, **48**(10): 794-811.
https://doi.org/10.5006/1.3315878

[51] Cheng YF, Luo JL and Wilmott M. Spectral analysis of electrochemical noise with different transient shapes. Electrochimica Acta, 2000, **45**(11): 1763-1771.
https://doi.org/10.1016/S0013-4686(99)00406-5

[52] Wang X, Wang J, Fu C, *et al*. Determination of corrosion type by wavelet-based fractal dimension from electrochemical noise. International Journal of Electrochemical Science, 2013, **8**: 7211-7222.

[53] Suresh G and Mudali U K. Electrochemical noise analysis of pitting corrosion of type 304L stainless steel. Corrosion, 2013, **70**(3): 283-293.
https://doi.org/10.5006/1003

[54] Smith MT and Macdonald DD. Wavelet analysis of electrochemical noise data. Corrosion, 2009, **65**(7): 438-448.

[55] Attarchi M, Roshan MS, Norouzi S, *et al*. Electrochemical potential noise analysis of CuBTA system using wavelet transformation. Journal of Electroanalytical Chemistry, 2009, **633**(1): 240-245.
https://doi.org/10.1016/j.jelechem.2009.06.008

[56] Davoodi A, Pan J, Leygraf C, *et al*. Integrated AFM and SECM for in situ studies of localized corrosion of Al alloys. Electrochimica Acta, 2007, **52**(27): 7697-7705. https://doi.org/10.1016/j.electacta.2006.12.073

[57] Liu L, Li Y and Wang F. Pitting mechanism on an austenite stainless steel nanocrystalline coating investigated by electrochemical noise and in-situ AFM analysis. Electrochimica Acta, 2008, **54**(2): 768-780. https://doi.org/10.1016/j.electacta.2008.06.076

[58] Zhang Z, Leng WH, Cai QY, *et al*. Study of the zinc electroplating process using electrochemical noise technique. Journal of electroanalytical Chemistry, 2005, **578**(2): 357-367. https://doi.org/10.1016/j.jelechem.2005.01.029

[59] Cao FH, Zhang Z, Su JX, *et al*. Electrochemical noise analysis of LY12-T3 in EXCO solution by discrete wavelet transform technique. Electrochimica Acta, 2006, **51**(7): 1359-1364. https://doi.org/10.1016/j.electacta.2005.07.012

[60] Shahidi M, Hosseini SMA, Jafari AH. Comparison between ED and SDPS plots as the results of wavelet transform for analyzing electrochemical noise data. Electrochimica Acta, 2011, **56**(27): 9986-9997. https://doi.org/10.1016/j.electacta.2011.08.091

[61] Seo M, Hultquist G, Leygraf C, *et al*. The influence of minor alloying elements (Nb, Ti and Cu) on the corrosion resistivity of ferritic stainless steel in sulfuric acid solution. Corrosion Science, 1986, **26**(11): 949-960. https://doi.org/10.1016/0010-938X(86)90085-5